Enhancing Hydrogen Storage Capacity of Pd Nanoparticles by Sandwiching between Inorganic Nanosheets

Kevin Ament,[a, b] Hirokazu Kobayashi,[c] Kohei Kusada,[c, d] Josef Breu,*[a, b] and Hiroshi Kitagawa*[c]

Dedicated to Prof. Dr. Caroline Röhr on the Occasion of her 60th Birthday.

H_2 is regarded to play a crucial role in the transition from a fossil fuel-based energy economy towards an environmentally friendly one. However, storage of H_2 is still challenging, but palladium (Pd) based materials show exciting properties. Therefore, nanoparticulate Pd has been intensely studied for hydrogen storage in the past years. Here, we stabilize Pd nanoparticles by intercalation between inorganic nanosheets of hectorite (NaHec). Compared to nanoparticles stabilized by the polymer polyvinylpyrrolidone (PVP), the H_2 storage capacity was found to be 86% higher for identical Pd nanoparticles being intercalated between nanosheets. We attribute this remarkably enhanced H_2 storage capacity to the partial oxidation of Pd, as evidenced by X-ray photoelectron spectroscopy (XPS). The higher amount of holes in the *4d* band leads to a higher amount of H_2 that can be absorbed when Pd is stabilized between the nanosheets of hectorite compared to the PVP stabilized nanoparticles.

Introduction

H_2 is of industrial importance, e.g. for hydrogenation reactions, synthesis of ammonia or oil refining.[1] Furthermore, interest has emerged in hydrogen as a clean energy source, e.g. for fuel cells.[2] These applications require reliable storage of H_2. Materials with a high surface area that can bind H_2 physically, such as carbon materials (activated carbon, nanotubes, nanofibers)[3] or metal-organic frameworks[4] require typically low temperatures or high pressures.[5] Materials capable of binding hydrogen chemically are metal hydrides[6] (MgH_2) or complex hydrides[7] ($NaBH_4$), but these hydrides require high

[a] K. Ament, Prof. Dr. J. Breu
Bavarian Polymer Institute, University of Bayreuth,
Universitätsstraße 30, 95447 Bayreuth (Germany)
E-mail: josef.breu@uni-bayreuth.de

[b] K. Ament, Prof. Dr. J. Breu
Department of Chemistry, University of Bayreuth,
Universitätsstraße 30, 95447 Bayreuth (Germany)

[c] H. Kobayashi, K. Kusada, Prof. H. Kitagawa
Division of Chemistry, Graduate School of Science,
Kyoto University,
Kitashirakawa-Oiwakecho, Sakyo-ku, Kyoto 606-8502 (Japan)
E-mail: kitagawa@kuchem.kyoto-u.ac.jp

[d] K. Kusada
The Hakubi Center for Advanced Research,
Kyoto University,
Kitashirakawa-Oiwakecho, Sakyo-ku, Kyoto, 606-8502 (Japan)

Supporting information for this article is available on the WWW under https://doi.org/10.1002/zaac.202100370

temperatures to release H_2. Transition metals represent another interesting class of hydrogen storage materials as they possess a high density of states (DOS) near the Fermi level. Among them, Pd is known to absorb high volumes of H_2 at ambient pressure and temperature.[8] The amount of hydrogen that can be absorbed is closely related to holes in the *4d* band as the Pd–H bond is created by electron transfer of H *1s* electrons to these holes.[9]

Nanoparticles show significantly altered physical and chemical properties[10] compared to their bulk counterparts, such as improved catalytic activity[11] or melting point depression.[12] Nano-sizing and confinement was recognized for complex metal hydrides to improve hydrogen uptake properties.[13] When complex metal hydride nanoparticles were incorporated into the pores of SBA-15[14] or nanoporous carbon[15] not only stability of the nanoparticles, but also the kinetics of H_2 uptake and release or thermodynamic phase stabilities at given H_2 pressure and temperatures were changed.

The nano-size effect on the H_2 storage behaviour of Pd nanoparticles was thoroughly investigated applying polyvinylpyrrolidone (PVP) covered nanoparticles. The polymeric capping ligand inhibited agglomeration while allowing H_2 to access the surface.[16] Nanoparticles of Pd demonstrated a clear size-dependent effect.[17] With decreasing size, the maximum H_2 absorption decreases accompanied by a narrowing of the two-phase region (coexistence phase of α and β) compared to bulk Pd. Alternatively, the storage capacity of Pd nanoparticles was improved by tuning their electronic structure. In this line, the H_2 storage capacity of nanoparticulate Pd cubes could be doubled by covering them with the metal-organic framework (MOF) HKUST-1 (copper(II) 1,3,5-benzenetricarboxylate).[18] The improvement of H_2 storage capacity was rationalized by a charge transfer from the Pd nanocubes to Cu–O groups of the MOF, which increases the number of holes in the *4d* band.[9]

Recently, Pd nanoparticles were intercalated between the nanosheets of synthetic hectorite (NaHec, $Na_{0.5}Mg_{2.5}Li_{0.5}Si_4O_{10}F_2$). NaHec is a 2 dimensional (2D) 2:1 layered silicate. The synthetic procedure involving melt synthesis and thermal annealing grants access to a phase pure material with a 3 dimensional crystalline order.[19] This makes the material more favourable for systematic studies over natural materials as it possess little defects and no impurities. Furthermore, the synthetic hectorite is a fluorohectorite. This renders this clay structure stable up to 750 °C.[20] As the silicate nanosheets carry a high permanent negative charge Na^+ ions are located between these nanosheets to grant charge balance.[19b] When immersed in water, the nanosheets delaminate by repulsive osmotic swelling into individual nanosheets with a thickness of 9.6 Å.[21] The electrostatic repulsion and a large diameter of ≈20000 nm hold the nanosheets in a co-facial alignment even at high dilutions, forming a nematic liquid crystalline phase. This nematic phase was used to intercalate nanoparticles with a positive ζ potential between the nanosheets to create a porous structure as sketched in Scheme S1.[22] The confinement between negatively charged nanosheets forces the Pd nanoparticles to be positively charged to balance the charge. Furthermore, the nanosheets even accept additional negative charge beyond what is expected for charge balancing of pristine NaHec as evidenced by electron energy loss spectroscopy (EELS) of Si.[22] Similar to what was reported for HKUST-1 embedded Pd nanoparticles, we find that the additional holes created by the described charge transfer for intercalated nanoparticulate Pd indeed also enhances the maximum H_2 storage capacity compared to identical nanoparticles covered with PVP.

Results and Discussion

Crystalline NaHec was delaminated in water to form a 1.5 wt% nematic sol. At this solid content, individual nanosheets were separated to about 60 nm according to small-angle X-ray scattering (SAXS, Figure S1). Pd nanoparticles with a positive ζ potential were synthesized by reducing $Na_2[PdCl_4]$ in the presence of 4-dimethylaminopyridine (DMAP).[23] The as-synthesized nanoparticles had a core size of 3.5 ± 0.4 nm as determined by transmission electron microscopy (TEM, Figure S2a,b). The hydrodynamic diameter was found to be 4.5 ± 1.3 nm applying dynamic light scattering (DLS, Figure S2c). As the layer charge of the NaHec nanosheets is fixed due to the isomorphous substitution of Li^+ for Mg^{2+}, the number of nanoparticles that can be intercalated between the nanosheets can be controlled by the pH-dependent surface charge of the nanoparticles. The ζ potential of the nanoparticles could be systematically varied by pH adjustment between 28 mV and 34 mV at a pH of 9.5 and 6.0, respectively (Figure S3). Typically, a 1.0 wt% dispersion of the Pd nanoparticles was added to a 1.5 wt% dispersion of the nematic sol of Hec under vigorous stirring. After flocculation of the oppositely charged species, the composite was repeatedly centrifuged and washed. The amount of Pd captured by NaHec was determined by energy-dispersive X-ray spectroscopy (EDS). At a pH of 6.0, the Pd

weight fraction was 39.3% (Hec@Pd39@Hec), whereas at pH 9.5, the amount of Pd was as high as 64.5 wt% (Hec@Pd65@Hec). The amount of Na^+ was below the detection limit of EDS. XPS of Na *1s* region did not show a signal of remaining Na^+. In contrast, a clear signal was visible for pristine NaHec (Figure S4). According to CHN analysis, the DMAP capping ligand was completely removed during the washing steps suggesting that positively charged Pd nanoparticles solely guarantee the charge balance. This was cross checked by XPS analysis of the N *1s* region showing no signal of residuals of the nitrogen-containing ligand (Figure S4b).

TEM images of both samples showed that the nanoparticles were captured between the nanosheets. Hec@Pd39@Hec had a disordered structure with collapsed areas. At this low pH, the Pd nanoparticles carry a high positive ζ potential and consequently, very few nanoparticles were required to balance the negative surface charge. In turn, adjacent nanoparticles are too distant to keep the gallery between nanosheets open. The flexible nanosheets[24] completely encapsulated individual nanoparticles (Figure 1a). Since the nanosheets are impermeable for H_2,[25] the Pd nanoparticles at this low loading turned out to be not accessible for CO chemisorption or Ar (Figure S5a). More nanoparticles that are closer to each other were required to prevent the nanosheets from collapsing. When the surface charge of the nanoparticles was lowered by increasing the pH to 9.5, and consequently, more nanoparticles were intercalated to achieve charge balance, an ordered lamellar structure was obtained (Figure 1b). The nanoparticles are sandwiched between two nanosheets while the gallery is kept open by sufficient nanoparticles serving as pillars (Figure 1c). Upon intercalation, the nanoparticles retained their size of 3.5 ±
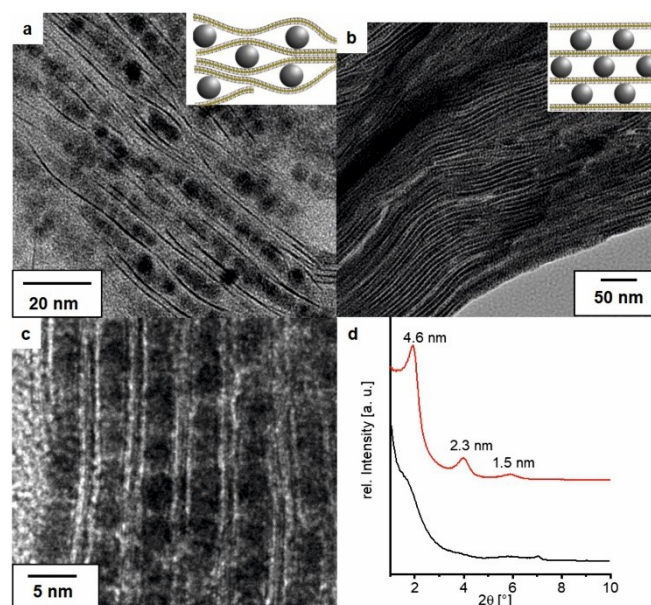

Figure 1. Structural characterization of Hec@Pd39@Hec and Hec@Pd65@Hec: a) TEM image of Hec@Pd39@Hec. b, c) TEM images of Hec@Pd65@Hec. d) PXRD at low angles of Hec@Pd39@Hec (black) and Hec@Pd65@Hec (red).

0.4 nm. This was confirmed at larger length scales as compared to TEM images by Powder X-ray diffraction (PXRD, Figure 1d). In line with the disorder apparent in TEM images, Hec@Pd39@Hec showed only a broad shoulder at low angles due to a random interstratification of occupied and unoccupied interlayer spaces. In contrast, for Hec@Pd65@Hec a series of reflections (*00l* series) was observed with a *d* spacing of 4.6 nm. This is in excellent agreement with the sum of a typical nanoparticle sized 3.4 nm and the 0.96 nm thick nanosheet. Furthermore, the coefficient of variation of 0.78% proved a rational series and a high degree of order along the stacking direction indicating a quite uniform *d* spacing.

Hec@Pd65@Hec was found to be mesoporous with a BET surface of 163 m^2/g and a median pore size of 4.5 nm, suggesting that the Pd nanoparticles are not densely packed (Figure S5). The metal dispersion, determined by CO chemisorption, was 24%, demonstrating that the nanoparticles were accessible. In contrast, the BET surface of Hec@Pd39@Hec was as low as 18 m^2/g, and chemisorption was below the detection limit.

Pressure-composition (PC) isotherms were acquired for Hec@Pd39@Hec and Hec@Pd65@Hec at 303 K (Figure 2). Furthermore, the DMAP covered Pd nanoparticles were stabilized with PVP as the polymer is regarded to take no influence on uptake behaviour.[17] The nanoparticles retained their size upon capping ligand exchange (Figure S6), and the metal content was 10.1 wt%, according to elemental analysis. The reference is denoted as PdPVP. Before the measurement, the samples were evacuated at 423 K for 6 h. Hec@Pd39@Hec did not absorb hydrogen, which proved that even the very small H_2 molecules could not diffuse between the collapsed nanosheets and access the encapsulated Pd nanoparticles. Only some external Pd could absorb small amounts of H. The H_2 uptake at 101 kPa H_2 pressure of the reference PdPVP nanoparticles was 0.35 H/Pd showing – as expected for such small nanoparticles- a clear nanosize effect compared to Pd black (~0.7 H/Pd) and the reduction observed here is in good accordance with the literature.[17] For Hec@Pd65@Hec, the amount of absorbed H

increased with increasing H_2 pressure. At 101 kPa, Hec@Pd65@-Hec absorbed 0.65 H/Pd. This was an increase of 86% compared to the 0.35 H/Pd of PdPVP. Additionally, the plateau-like region, where the solid solution of Pd and H (α-phase) and the hydride formation (β-phase) coexist, is more pronounced compared to PdPVP. As the same nanoparticles were used for the synthesis of Hec@Pd65@Hec as well as PdPVP, the sandwich confinement by the Hec nanosheets seems to have impact on the H_2 uptake. Furthermore, while for sterically stabilized PdPVP the complete metal surface is accessible, for Hec@Pd65@Hec as little as 24% of the Pd atoms were measured to be accessible by CO chemisorption. When comparing the specific hydrogen densities of Hec@Pd65@Hec and PdPVP of 0.4 wt% and 0.03 wt%, respectively, the difference in the H_2 uptake is even higher due to higher density of Pd nanoparticles in Hec@Pd65@Hec. Nevertheless, the specific hydrogen density is lower compared to Pd black as it consists of 35 wt% Hec- support.

To clarify whether the increased uptake of H_2 of Hec@Pd65@Hec was a spillover effect to the Hec support or absorbed into the lattice of Pd, *in situ* diffraction measurements at variable H_2 pressure were performed. The transition from α to β phase is a first-order transition[26] and is accompanied by an expansion of the Pd lattice.[27] The change in the position of the *fcc* diffraction peaks of Pd was recorded *in situ* at various hydrogen pressures at Super Photon Ring SPring-8 (Figure 3a).[28] From vacuum to 1 kPa, the *fcc* peaks of Pd only gradually shifted to lower angles corresponding to the solid solution of the α-phase. The transition appeared in a very narrow pressure range, and peaks completely shifted to lower angles already at 2 kPa and shifted back at 0.5 kPa during the desorption process. Le Bail fitting of the diffraction patterns proved that the lattice constant of Pd increased with hydrogen pressure and decreased when the hydrogen desorbed again (Figure 3b). The lattice constant returned to its original value after desorption, proving complete reversibility. It should be noted that the lattice was able to expand even though the
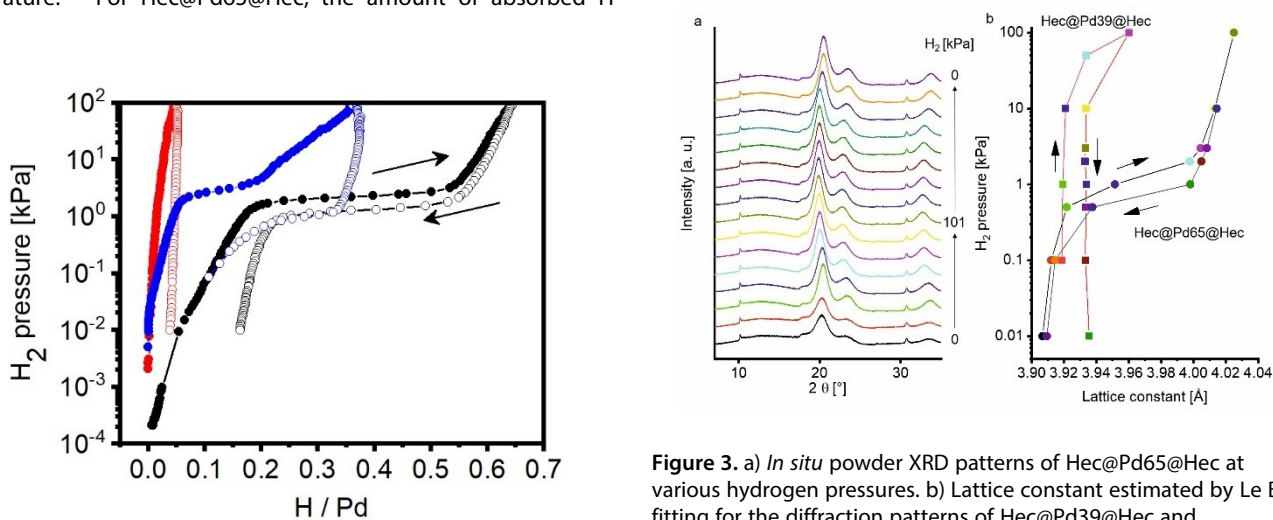

Figure 2. PC isotherms at 303 K of Hec@Pd39@Hec (red), Hec@Pd65@Hec (black), and PdPVP (blue).

Figure 3. a) *In situ* powder XRD patterns of Hec@Pd65@Hec at various hydrogen pressures. b) Lattice constant estimated by Le Bail fitting for the diffraction patterns of Hec@Pd39@Hec and Pd@65@Hec. The colour code of the diffraction patterns corresponds to the lattice constant in a). The diffraction patterns of Hec@Pd39@Hec can be found in Figure S7.

nanoparticles were sandwiched between the silicate nano-sheets. The change in the lattice constant upon H_2 pressure is fully consistent with the course of the PC isotherm plotted in Figure 2 which is a good hint that H_2 uptake is due to the sorption into the lattice of Pd nanoparticles rather than a spillover process.

As expected, the lattice constant of Hec@Pd39@Hec hardly shifted upon the insignificant hydrogen uptake (Figure 3b and S7).

XP spectra of the Pd *3d* region of Hec@Pd39@Hec and Hec@Pd65@Hec were recorded to investigate the influence of hectorite on the electronic structure of Pd nanoparticles (Figure 4). The signals of Hec@Pd65@Hec were fitted with a pair of asymmetric bands ($3d_{5/2}$ and $3d_{3/2}$) with a spin orbit coupling of 5.26 eV characteristic for Pd metal (Figure S8). The binding energies (BE) of Pd $3d_{5/2}$ was 335.8 eV for Hec@Pd65@Hec, considerably shifted to higher values than the 335.0 eV of bulk Pd.[29] As the DMAP capped nanoparticles of Hec@Pd39@Hec had a higher ζ potential at synthesis, the Pd $3d_{5/2}$ signal at this stage was at 336.0 eV. In contrast, Pd $3d_{5/2}$ of PdPVP was found at a BE of 335.1 eV. The shift to higher BE values suggested that Hec covered nanoparticles were in a different electronic state from the PVP covered nanoparticles and were slightly electron-deficient. The negatively charged nanosheets forced the nano-particles to be in a positively charged state. Furthermore, a charge transfer from Pd to the Si of the nanosheets was reported before.[22] The amount of hydrogen that can be absorbed strongly correlates with the amount of *4d* band holes in the conduction band at the Fermi level.[30] Based on the band filling effect, the more holes in the *4d* band, the more hydrogen can be absorbed as the transfer of H *1s* electrons into these holes creates the Pd–H bonds.[31] Similar behaviour was also found for metal alloys of Pd–Ir[32] or Pd–Rh,[33] where a charge transfer from Pd to the other metal increased the number of

holes and total H_2 storage capacity. Furthermore, covering Pd nanocubes with HKUST-1 doubled the hydrogen uptake due to charge transfer from Pd to Cu–O centres.[9,18] In the same line, we propose that the electron-deficient Pd species created by intercalation between NaHec nanosheets can absorb more hydrogen due to an increased amount of holes in the *4d* band.

Conclusions

The results demonstrate that the amount of hydrogen absorbed by Pd nanoparticles can be significantly altered by intercalation between the permanently negatively charged 2D layered material hectorite. The nanosheets influence the electronic structure of the nanoparticles and thus modulate the amount of hydrogen that can be absorbed. Furthermore, it was shown that a proper adjustment of the ζ potential of the nanoparticles before intercalation was crucial to obtain mesoporous materials with Pd surfaces being accessible. The findings show that confinement between the Hec nanosheets can improve the H_2 storage capacity by alteration of the electronic structure. As the intercalation strategy can most likely be applied to other nanoparticulate materials, storage capacity of more abundant and cheaper nanoparticles might be tunable on the way to reliable and affordable H_2 storage materials.

Experimental Section

Materials

$PdCl_2$ (99.999% Pd, Premion), NaCl, 4-Dimethylaminopyridine (DMAP), NaOH, NaCl and $NaBH_4$ were purchased from Alfa Aesar. Polyvinylpyrrolidone (PVP) with an average mol wt of 40000 was purchased from Sigma Aldrich. The used water was of MilliQ quality (18.2 MΩ).

Synthesis of Pd nanoparticles

The synthesis of Pd nanoparticles was executed using a modified literature procedure.[23] Palladium (II) chloride (235 mg, 1.33 mmol) and Sodium chloride (155 mg, 2.66 mmol) were dissolved in 40 mL water and 4-Dimethylaminopyridine DMAP (833 mg, 6.82 mmol) in 80 mL water was added. After 20 min of stirring $NaBH_4$ (110 mg, 2.91 mmol) in 11 mL water was added dropwise under vigorous stirring resulting in a black dispersion. After 2 h the nanoparticle dispersion was dialyzed in 4 L water with water changes after 12 and 24 hours.

Synthesis of NaHec

NaHec was synthesized via melt synthesis and is described elsewhere.[19b]

Synthesis of Hec@Pd@Hec

For the synthesis of the composite materials the hectorite was delaminated to a 1.5 wt% dispersion to achieve a layer distance of about 60 nm. Both the aqueous nanoparticle and hectorite dispersions were adjusted resulting in surface potentials of the
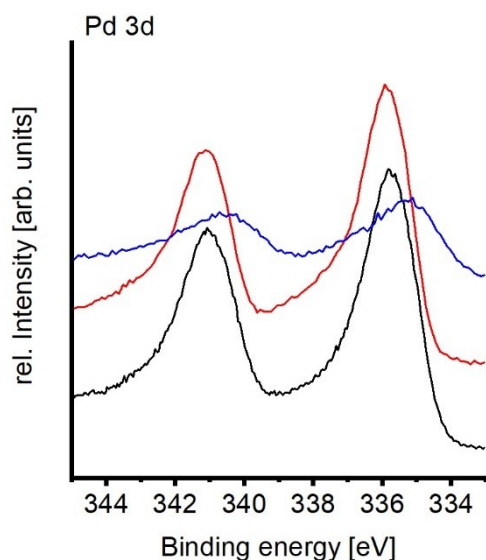

Figure 4. XP spectra of Pd *3d* region of Hec@Pd65@Hec (black), Hec@Pd39@Hec (red), and PdPVP (blue).

nanoparticles of 28 mV or 34 mV, respectively. The nematic hectorite suspension was added rapidly to the nanoparticle dispersion under vigorous stirring. Visible flocculation appeared within 30 seconds. The black flocculate was separated from the supernatant by centrifugation. DMAP was removed by three washing cycles. Finally, the material was freeze-dried to obtain a fluffy powder.

Synthesis of PdPVP

Nanoparticles were covered with PVP by a ligand exchange process. To about 100 mg of DMAP capped Pd nanoparticles in aqueous dispersion (100 mL) was added 900 mg PVP. The dispersion was stirred for 2 days and the dispersion was then dialyzed in 4 L water with water changes after 12 and 24 hours. The material was dried at 130 °C.

Characterization

Dynamic light scattering (DLS) and determination of ζ-potential were recorded on a Litesizer 500 (Anton-Paar).

CHN analysis was acquired with an Elementar Vario EL III.

PXRD of traces of textured samples were recorded on a Bragg-Brentano type diffractometer (Empyrean, PANalytical) with nickel filter and $Cu_{K\alpha}$ radiation ($\lambda = 1.54187$ Å).

SAXS data were measured using a "Double Ganesha AIR "system (SAXSLAB,Denmark). The X-ray source of this laboratory-based system is a rotating anode (copper, MicroMax 007HF, Rigaku Corporation, Japan) providing a microfocused beam. The data is recorded by a position sensitive detector (PILATUS 300 K, Dectris).

Transmission electron microscopy (TEM) images were acquired using a JEOL JEM-2200FS (200 kV). For cross sectional TEM the powder was embedded into a resin (EPO-TEK 301) and was cut with an Ar beam into thin slices using a Jeol Cryo Ion Slicer.

Scanning electron microscopy (SEM) images and energy dispersive spectroscopy (EDS) were recorded on a FEI Quanta FEG 250.

Photoelectron spectroscopy (XPS) was conducted on a Versa Probe III fitted with an Al K_{α} source. Spectra were referenced to C 1s at 284.8 eV.

Adsorption isotherms were recorded on a Quantachrome Autosorb-1 with Ar as adsorbate at 87 K. The isotherms were evaluated using Brunauer-Emmet-Teller (BET) method and pore size distribution was evaluated with NLDFT.

Metal surface was acquired via CO chemisorption with a Quantachrome Autosorb-1 using the double isotherm method at 35 °C.

PC isotherm measurements were acquired using a pressure-temperature apparatus (BEL JAPAN). Before measurement all samples were activated at 423 K under vacuum for 6 h. PC isotherms were measured from 10^{-3} up to 101 kPa hydrogen pressure at 303 K. The adsorption/desorption process was repeated at least for three times to eliminate the possibility of surface oxide contamination.

In situ XRD measurements were acquired at Beamline BL02B2 at SPring-8. Samples were sealed in a glass capillary and were measured under controlled hydrogen pressure in the range from 0 to 101 kPa at 303 K. The radiation wave length was 0.8 Å and the step size was 0.006°.

Conflict of Interest

The authors declare no conflict of interest.

Data Availability Statement

Research data are not shared.

[1] S. Dunn, *Int. J. Hydrogen Energy* **2002**, *27*, 235–264.
[2] L. Schlappbach, A. Züttel, *Nature* **2001**, *414*, 353–358.
[3] W. C. Xu, K. Takahashi, Y. Matsuo, Y. Hattori, M. Kumagai, S. Ishiyama, K. Kaneko, S. Iijima, *Int. J. Hydrogen Energy* **2007**, *32*, 2504–2512.
[4] M. P. Suh, H. J. Park, T. K. Prasad, D.-W. Lim, *Chem. Rev.* **2012**, *112*, 782–835.
[5] S. Dekura, H. Kobayashi, K. Kusada, H. Kitagawa, *ChemPhysChem* **2019**, *20*, 1158–1176.
[6] N. A. A. Rusman, M. Dahari, *Int. J. Hydrogen Energy* **2016**, *41*, 12108–12126.
[7] S.-i. Orimo, Y. Nakamori, J. R. Eliseo, A. Züttel, C. M. Jensen, *Chem. Rev.* **2007**, *107*, 4111–4132.
[8] a) F. D. Manchester, A. San-Martin, J. M. Pitre, *J. Phase Equilib.* **1994**, *15*, 62–83; b) H. Kobayashi, M. Yamauchi, H. Kitagawa, Y. Kubota, K. Kato, M. Takata, *J. Am. Chem. Soc.* **2008**, *130*, 1828–1829.
[9] Y. Chen, O. Sakata, Y. Nanba, L. S. R. Kumara, A. Yang, C. Song, M. Koyama, G. Li, H. Kobayashi, H. Kitagawa, *Commun. Chem.* **2018**, *1*, 61.
[10] E. Roduner, *Chem. Soc. Rev.* **2006**, *35*, 583–592.
[11] a) A. S. K. Hashmi, G. J. Hutchings, *Angew. Chem. Int. Ed.* **2006**, *45*, 7896–7936; *Angew. Chem.* **2006**, *118*, 8064–8105; b) D. Astruc, *Chem. Rev.* **2020**, *120*, 461–463.
[12] a) P. Schlexer, A. B. Andersen, B. Sebok, I. Chorkendorff, J. Schiøtz, T. W. Hansen, *Part. Part. Syst. Charact.* **2019**, *36*, 1800480; b) P. Buffat, J. P. Borel, *Phys. Rev. A* **1976**, *13*, 2287–2298.
[13] P. E. de Jongh, P. Adelhelm, *ChemSusChem* **2010**, *3*, 1332–1348.
[14] P. Ngene, P. Adelhelm, A. M. Beale, K. P. de Jong, P. E. de Jongh, *J. Phys. Chem. C* **2010**, *114*, 6163–6168.

[15] J. Gao, P. Adelhelm, M. H. W. Verkuijlen, C. Rongeat, M. Herrich, P. J. M. van Bentum, O. Gutfleisch, A. P. M. Kentgens, K. P. de Jong, P. E. de Jongh, *J. Phys. Chem. C* **2010**, *114*, 4675–4682.

[16] a) H. Tsunoyama, H. Sakurai, Y. Negishi, T. Tsukuda, *J. Am. Chem. Soc.* **2005**, *127*, 9374–9375; b) N. J. J. Johnson, B. Lam, R. S. Sherbo, D. K. Fork, C. P. Berlinguette, *Chem. Mater.* **2019**, *31*, 8679–8684.

[17] M. Yamauchi, R. Ikeda, H. Kitagawa, M. Takata, *J. Phys. Chem. C* **2008**, *112*, 3294–3299.

[18] G. Li, H. Kobayashi, J. M. Taylor, R. Ikeda, Y. Kubota, K. Kato, M. Takata, T. Yamamoto, S. Toh, S. Matsumura, H. Kitagawa, *Nat. Mater.* **2014**, *13*, 802–806.

[19] a) H. Kalo, W. Milius, J. Breu, *RSC Adv.* **2012**, *2*, 8452–8459; b) M. Stöter, D. A. Kunz, M. Schmidt, D. Hirsemann, H. Kalo, B. Putz, J. Senker, J. Breu, *Langmuir* **2013**, *29*, 1280–1285.

[20] K. Ament, D. R. Wagner, F. E. Meij, F. E. Wagner, J. Breu, *Z. Anorg. Allg. Chem.* **2020**, *646*, 1110–1115.

[21] S. Rosenfeldt, M. Stöter, M. Schlenk, T. Martin, R. Q. Albuquerque, S. Förster, J. Breu, *Langmuir* **2016**, *32*, 10582–10588.

[22] K. Ament, N. Köwitsch, D. Hou, T. Götsch, J. Kröhnert, C. J. Heard, A. Trunschke, T. Lunkenbein, M. Armbrüster, J. Breu, *Angew. Chem. Int. Ed.* **2021**, *60*, 5890–5897; *Angew. Chem.* **2021**, *133*, 5954–5961.

[23] K. A. Flanagan, J. A. Sullivan, H. Müeller-Bunz, *Langmuir* **2007**, *23*, 12508–12520.

[24] D. A. Kunz, J. Erath, D. Kluge, H. Thurn, B. Putz, A. Fery, J. Breu, *ACS Appl. Mater. Interfaces* **2013**, *5*, 5851–5855.

[25] C. Habel, E. S. Tsurko, R. L. Timmins, J. Hutschreuther, R. Kunz, D. D. Schuchardt, S. Rosenfeldt, V. Altstädt, J. Breu, *ACS Nano* **2020**, *14*, 7018–7024.

[26] a) R. Bardhan, L. O. Hedges, C. L. Pint, A. Javey, S. Whitelam, J. J. Urban, *Nat. Mater.* **2013**, *12*, 905–912; b) A. Baldi, T. C. Narayan, A. L. Koh, J. A. Dionne, *Nat. Mater.* **2014**, *13*, 1143–1148; c) S. Syrenova, C. Wadell, F. A. A. Nugroho, T. A. Gschneidtner, Y. A. Diaz Fernandez, G. Nalin, D. Świtlik, F. Westerlund, T. J. Antosiewicz, V. P. Zhdanov, K. Moth-Poulsen, C. Langhammer, *Nat. Mater.* **2015**, *14*, 1236–1244.

[27] M. Yamauchi, H. Kobayashi, H. Kitagawa, *ChemPhysChem* **2009**, *10*, 2566–2576.

[28] E. Nishibori, M. Takata, K. Kato, M. Sakata, Y. Kubota, S. Aoyagi, Y. Kuroiwa, M. Yamakata, N. Ikeda, *Nuclear Instruments and Methods in Physics Research Section A: Accelerators, Spectrometers, Detectors and Associated Equipment* **2001**, *467–468*, 1045–1048.

[29] a) R. Arrigo, M. E. Schuster, S. Abate, S. Wrabetz, K. Amakawa, D. Teschner, M. Freni, G. Centi, S. Perathoner, M. Havecker, R. Schlögl, *ChemSusChem* **2014**, *7*, 179–194; b) N. S. Babu, N. L. Lingaiah, R. Gopinath, P. S. S. Reddy, P. S. S. Prasad, *J. Phys. Chem. C* **2007**, *111*, 6447–6453.

[30] a) D. A. Papaconstantopoulos, B. M. Klein, E. N. Economou, L. L. Boyer, *Phys. Rev. B* **1978**, *17*, 141–150; b) G. Alefeld, *Hydrogen in Metals II*, Sprigner: Berlin, Heidelberg, **1978**.

[31] E. Wicke, H. Brodowsky, H. Züchner, in *Hydrogen in metals II*, Springer: Berlin, Heidelberg, **1978**, pp. 73–155.

[32] H. Kobayashi, M. Yamauchi, R. Ikeda, T. Yamamoto, S. Matsumura, H. Kitagawa, *Chem. Sci.* **2018**, *9*, 5536–5540.

[33] H. Kobayashi, H. Morita, M. Yamauchi, R. Ikeda, H. Kitagawa, Y. Kubota, K. Kato, M. Takata, S. Toh, S. Matsumura, *J. Am. Chem. Soc.* **2012**, *134*, 12390–12393.